ARMY RESEARCH LABORATORY

Tensile and Laterally Confined Compression Properties of Various 3-Dimensional (3-D) Woven Composites

by Mark Pankow, Ashiq Quabili, Stephen Whittie, and Chian Yen

ARL-TR-7143 **November 2014**

NOTICES

Disclaimers

The findings in this report are not to be construed as an official Department of the Army position unless so designated by other authorized documents.

Citation of manufacturer's or trade names does not constitute an official endorsement or approval of the use thereof.

Destroy this report when it is no longer needed. Do not return it to the originator.

Army Research Laboratory
Aberdeen Proving Ground, MD 21005-5069

ARL-TR-7143 **November 2014**

Tensile and Laterally Confined Compression Properties of Various 3-Dimensional (3-D) Woven Composites

Mark Pankow
NC State University

Ashiq Quabili
SURVICE Engineering Co.

Stephen Whittie
Oak Ridge Institute for Science and Education

Chian Yen
Weapons and Materials Research Directorate, ARL

REPORT DOCUMENTATION PAGE	Form Approved OMB No. 0704-0188

1. REPORT DATE *(DD-MM-YYYY)*	2. REPORT TYPE	3. DATES COVERED (From - To)
November 2014	Final	December 2013

4. TITLE AND SUBTITLE
Tensile and Laterally Confined Compression Properties of Various Three-Dimensional (3-D) Woven Composites

5a. CONTRACT NUMBER

5b. GRANT NUMBER

5c. PROGRAM ELEMENT NUMBER

6. AUTHOR(S)
Mark Pankow, Ashiq Quabili, Stephen Whittie, and Chian Yen

5d. PROJECT NUMBER
H84

5e. TASK NUMBER

5f. WORK UNIT NUMBER

7. PERFORMING ORGANIZATION NAME(S) AND ADDRESS(ES)
US Army Research Laboratory
ATTN: RDRL-WMM-B
Aberdeen Proving Ground, MD 21005-5069

8. PERFORMING ORGANIZATION REPORT NUMBER
ARL-TR-7143

9. SPONSORING/MONITORING AGENCY NAME(S) AND ADDRESS(ES)

10. SPONSOR/MONITOR'S ACRONYM(S)

11. SPONSOR/MONITOR'S REPORT NUMBER(S)

12. DISTRIBUTION/AVAILABILITY STATEMENT
Approved for public release; distribution unlimited.

13. SUPPLEMENTARY NOTES

14. ABSTRACTTR-7143
The material responses of 6 different 3-dimensional (3-D) woven architectures have been evaluated in quasi-static mechanical testing. The 3-D woven architectures consist of S-glass fiber and Sc-15 epoxy matrix. The 2 mechanical experiments, tensile and laterally constrained compression tests, have been conducted on the 3-D woven specimens to evaluate their linear elastic responses and obtain mechanical properties along with observing progressive failure and ultimate failure. Two main conclusions can be made from these studies: 1) the 3-D orthogonal architectures offer the smallest reduction in in-plane properties for through-the-thickness reinforcement, and 2) the 3-D layer-to-layer architectures provide the largest amount of energy absorption characterized by stable failure modes that are not typically seen in the orthogonal and laminated architectures.

15. SUBJECT TERMS
3-D woven, through-the-thickness reinforcement, mechanical properties, tensile, compression, Z-fiber, elastic modulus

16. SECURITY CLASSIFICATION OF:			17. LIMITATION OF ABSTRACT	18. NUMBER OF PAGES	19a. NAME OF RESPONSIBLE PERSON
a. REPORT	b. ABSTRACT	c. THIS PAGE			Mark Pankow
Unclassified	Unclassified	Unclassified	UU	32	19b. TELEPHONE NUMBER (*Include area code*) 410-306-0732

Standard Form 298 (Rev. 8/98)
Prescribed by ANSI Std. Z39.18

Contents

List of Figures

List of Tables

Acknowledgments

The authors wish to acknowledge Seth Ghiorse, Paul Moy, Tim Walter, Art Yiournas, and Jordan Wagner for their valuable feedback and assistance with experimental setups. The authors also wish to thank Textile Engineering and Manufacturing (T.E.A.M), Inc., for supplying the 3e-dimensional woven preforms and Jim Wolbert for fabricating the panels.

1. Introduction

A common issue with traditional laminated “layered” fiber-reinforced composites is that they often fail in delamination. Developing alternative methods such as stitching,[1,2] z-pinning,[3–5] and 3-dimensional (3-D) weaving[6] has been suggested as means to improve delamination resistance. In textile composites, both stitching and z-pinning[7] can induce damage in the fiber tows through the mechanical insertion of the reinforcements.[3] On the other hand, 3-D weaving benefits from the fact that the material is woven integrally, which limits the induced damage and likely eliminates delamination. While the weaving process may damage the fiber filaments due to passage through the loom, the insertion of matrix material redistributes the stress and minimizes the degradation of the mechanical properties.[8,9] There are many different types of proposed 3-D woven architectures[10] and these have been discussed in detail previously along with benefits and limitations.[11] A 3-D woven structure can be constructed in various ways such as orthogonal (Z-fiber) weave, layer-to-layer, and angle interlock. Figure 1 provides an example of 2 different types of 3-D woven structures: a) orthogonal weave and b) layer-to-layer. In this figure, the paths of the weft, warp, and Z-fibers are correspondingly represented as red, blue, and yellow colors.

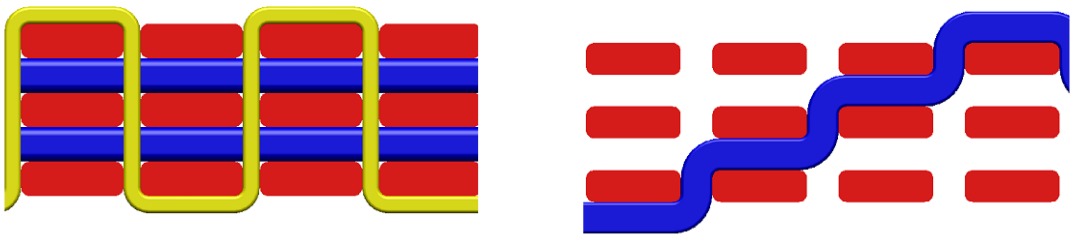

Fig. 1 Schematic of 3-D woven architecture cross sections

Two different experimentations were conducted on 6 distinct 3-D woven architectures to determine the architectural effect on mechanical properties. The first experiment was a tensile test to establish the modulus and strength of the architectures. A postfailure analysis was performed to determine any architecture-related features that could be identified. The second experiment was a laterally confined compression (LCC) test to determine the effective through-the-thickness response of the material. These results will be used to compare the resistance with penetration of the material.

Applications of 3-D textile composites include boat hulls, armor, and numerous possible future proposed implementations.[12] However, in-depth knowledge of the material properties, mechanical response, weave architecture dependency, and performance characteristics are ongoing subjects of research.

2. Specimen Configurations

The 6 different 3-D woven architectures described in this report were originally designed by the US Army Research Laboratory (ARL). The design specifications were provided to a textile weaver, T.E.A.M, Inc., for preform fabrications as a part of cooperative agreement between ARL and T.E.A.M. The 3-D woven architecture properties were compared and evaluated with plain weave 2-D samples (Base). An analysis of the yarn fraction in each orientation is shown in Table 1. The 3-D architecture configurations and the Base configuration are briefly described by the following:

- 3% Z-fiber: In this orthogonal 3-D design, approximately 3% of the total fiber was used as warp weavers (Z-fibers, orthogonal to the in-plane fibers). The Z-fibers wove all the way from the top surface to the bottom surface to interlock the in-plane fibers.
- 6% Z-fiber: In this orthogonal 3-D design, approximately 6% of the total fiber used was warp weavers (Z-fibers, orthogonal to the in-plane fibers). The Z-fibers wove all the way from the top surface to the bottom surface to interlock in-plane fibers.
- 10% Z-fiber: In this orthogonal 3-D design, approximately 10% of the total fiber used was warp weavers (Z-fibers, orthogonal to the in-plane fibers). The Z-fiber wove all the way from the top surface to the bottom surface to interlock the in-plane fibers.
- 12° angle interlock: In this 3-D woven configuration, the warp weavers wove all the way from top surface to the bottom surface at ±12° angle to interlock the in-plane fibers. The ratio of warp to fill fiber used in this architecture is 0.486:0.514.
- 20° layer-to-layer: In this 3-D design, each warp weaver wove at ±20° to interlock 2 adjacent in-plane fiber layers.
- 60° layer-to-layer: In this 3-D design, each warp weaver wove at ±60° to interlock 2 adjacent in-plane fiber layers.
- Base: This 2-D laminate was fabricated using 10 layers of 250-yield, 24-oz/yd², 5 × 5 plain-woven roving S-2 glass with orthotropic layup $[0]_{10}$.

For each of the 3-D architectures, the in-plane fibers were made of 250-yield S-2 glass, and the warp weavers were made of 1,250-yield S-2 glass fibers. Figure 2 illustrates the parametric representative unit cells (RUCs) of the 3-D woven architectures as described. The warp weavers are shown as white in color while the in-plane fibers are shown as red and/or blue.

Table 1 Fiber volume fractions

Configuration	Warp (%)	Weft (%)	Z-fiber (%)
Base	50.0	50.0	…
3%	46.0	49.0	4.0
6%	45.0	48.0	7.0
10%	43.0	48.0	9.0
12°	49.0	51.0	…
20°	51.0	49.0	…
60°	50.0	50.0	…

Note: 2.0% was used as a surface weaver.

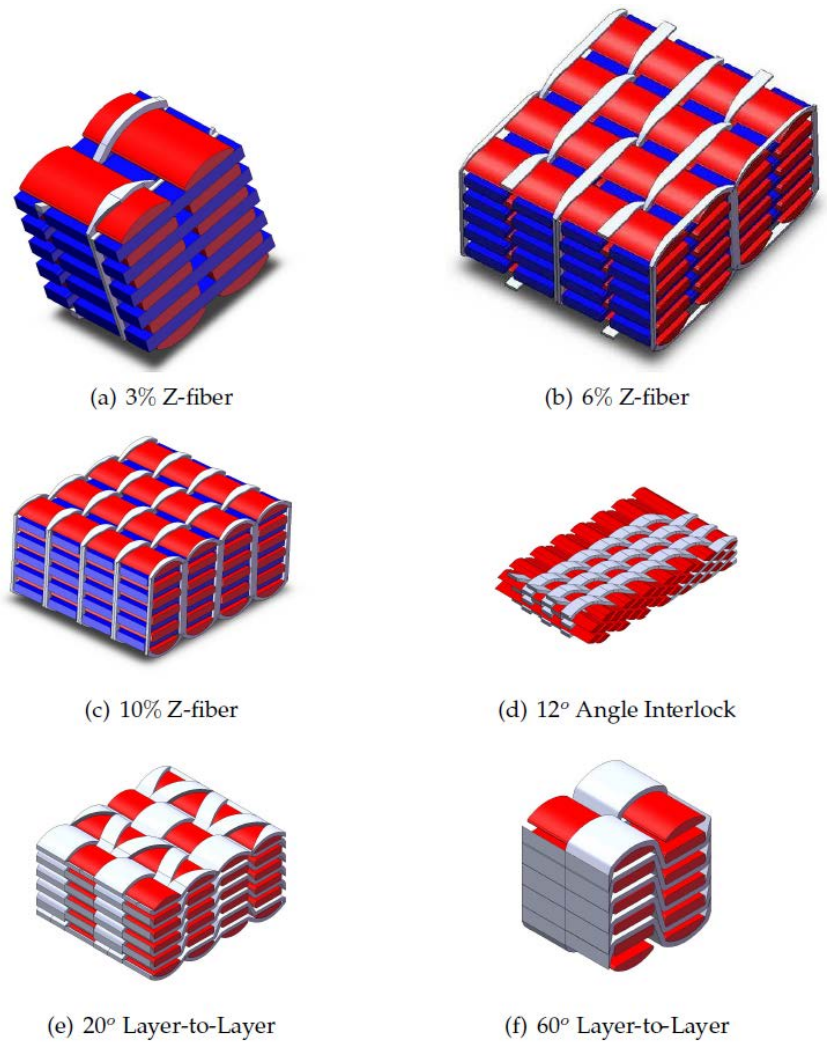

Fig. 2 RUC model shown for each of the 3-D woven architectures

3. Materials

3.1 Fiber

S-2 glass (AGY, Aiken, SC), used as the fibers in the weaving process, is a part of the magnesium-alumina-silicate-glass family of fibers. The individual properties under static loading are reported in Table 2.[13]

Table 2 S-2 glass fiber properties

E_{11} (GPa)	G_{12} (GPa)	ν_{12}
114.2	46.5	0.22

3.2 Matrix

SC-15 (Applied Poleramic, Inc., Benecia, CA), a thermosetting epoxy, was infused into the preforms. It is a low-viscosity 2-phased toughened epoxy resin system consisting of part A (resin mixture of diglycidylether epoxy toughener) and part B (hardener mixture of cycloaliphaic amine poluoxylalkylamine).[14] The mechanical properties of SC-15 are shown in Table 3. Also see Justusson et al.[15] for further characterization of the material including tension and compression.

Table 3 SC-15 matrix static properties

E_{11} (GPa)	ν_{12}	σ_u (MPa)	ε_u (%)
2.487	0.35	110	6.4

4. Fabrication and Void Content

4.1 Infusion

The panels were made using a vacuum-assisted resin transfer molding (VARTM) system. Figure 3 illustrates a schematic of VARTM process. There are many benefits to this process, some of which include shorter mold time, lower tooling costs, reduced volatile emissions, lower injection pressures, and the ability to do much larger structures.[16]

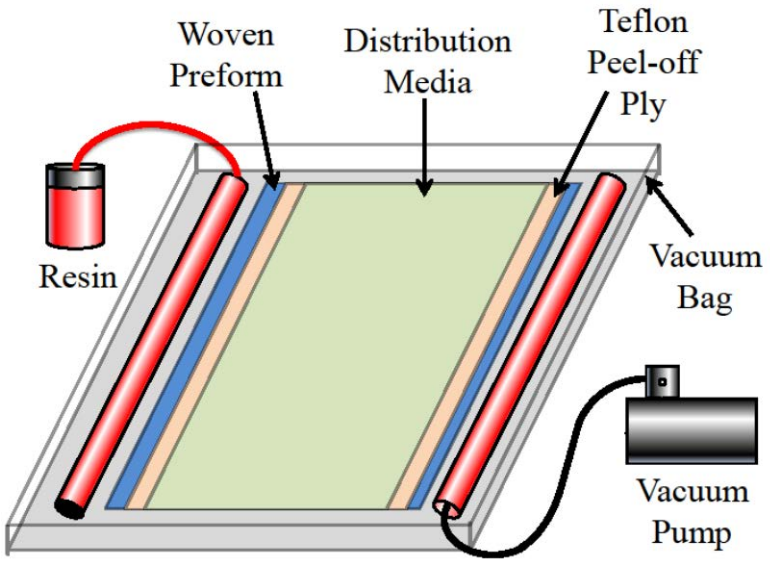

Fig. 3 Schematic of VARTM setup

4.2 Void Content

To determine the degree of impregnation, fiber burnout was performed to determine the void content of the specimens. This procedure is based on ASTM standard D2734.[17] The results of the burnout method are shown in Table 4, which indicates the volume fractions and densities. According to the calculations, the void content is within the manufactures specification. The postburnout images shown in Fig. 4 provide some details of the architectures and the movements of the Z-fiber in the different planes.

Table 4 Fiber volume fractions

Configuration	Fiber (%)	Matrix (%)	Voids (%)	Density (g/cc)
Base	47.1	50.5	2.4	1.744
3%	45.2	51.8	3.0	1.713
6%	45.9	53.5	0.6	1.749
10%	45.2	52.0	2.8	1.715
12°	41.6	57.6	0.8	1.689
20°	40.3	58.8	0.9	1.671
60°	39.2	57.4	3.4	1.627

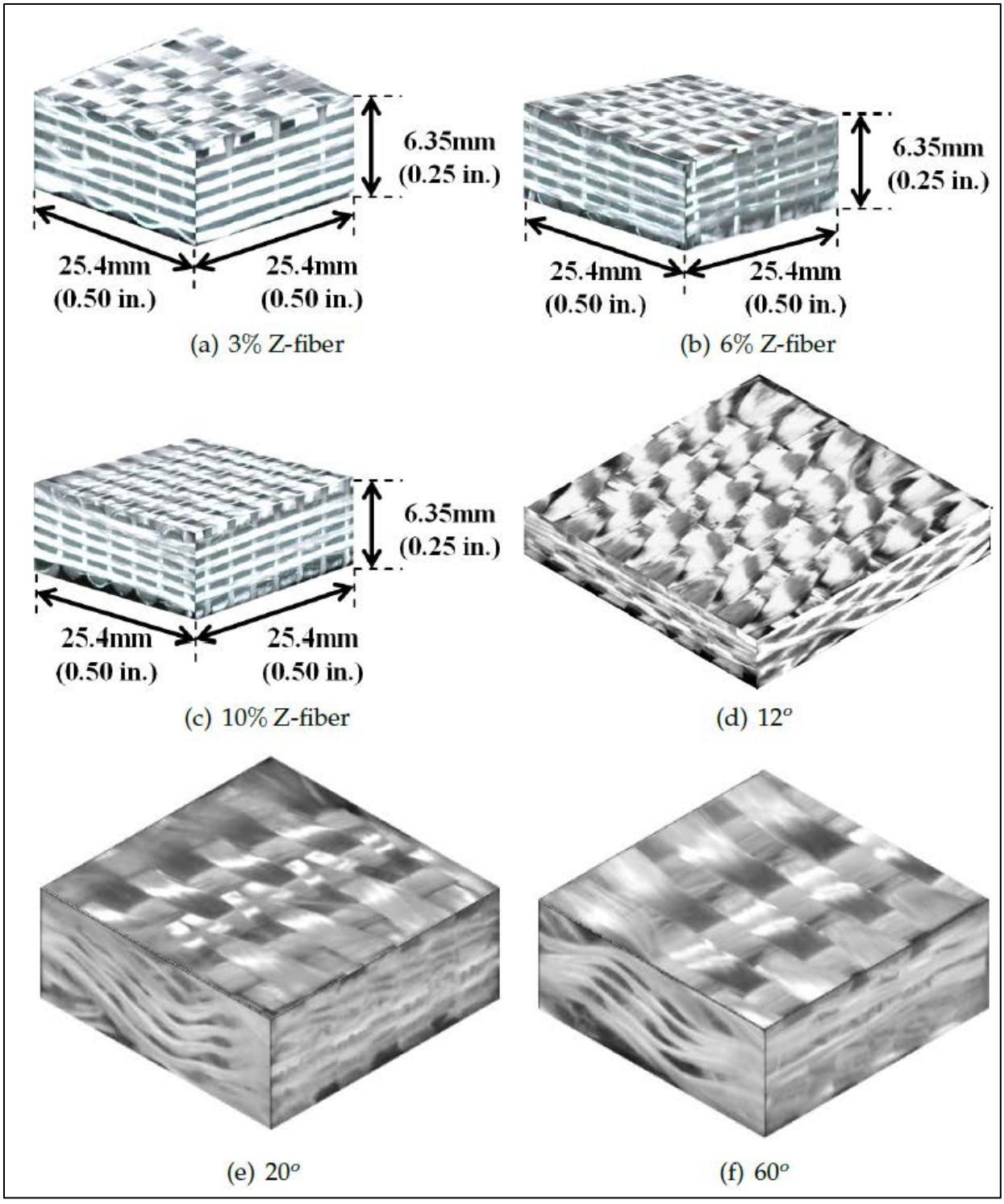

Fig. 4 Burnout scanned images of various 3-D woven composites

5. Experiment

The quasi-static tensile and LCC tests were performed on the 6 different 3-D architectures as previously described. The data represents the average of 5 specimens that were repeatedly tested in the exact configuration. Testing was performed with 3 different orientations: 0°, 45°, and 90°. The orientations are as indicated in Fig. 5. These different orientations give insight to the weft (0°) and warp (90°) response and the 45° orientation. The results were compared with plain-weave 2-D laminate properties.

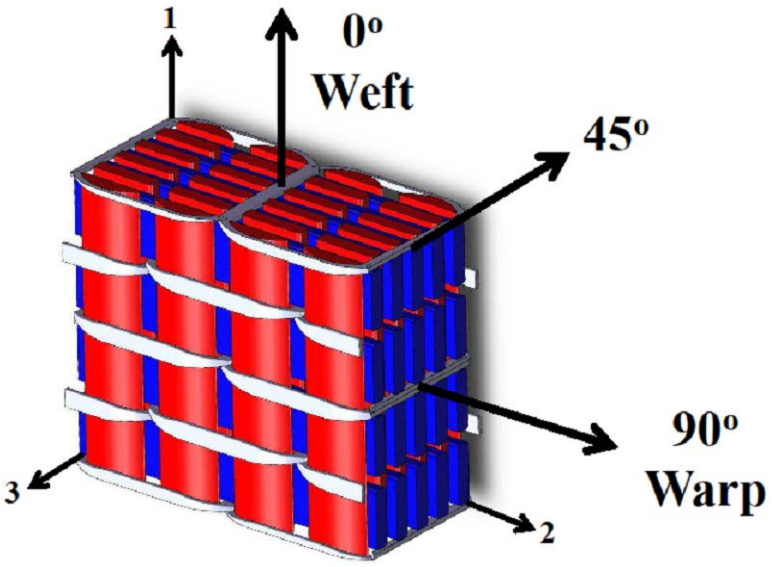

Fig. 5 Various in-plane material orientations for mechanical testing

5.1 Tensile Test

While 3-D weaving may cause some reduction in the in-plane mechanical properties, the reduction has historically been marginal (less than 5%).[8,9,18] Other researchers have shown that the mechanical properties are heavily dependent on the weaving architectures.[19] Some studies have specifically looked at how the Z-fiber will influence the failure path,[20] showing that the Z-fiber is typically a source of failure. It has been reported that the variances in weaving tensions could also affect the properties measured using tensile tests.[21] Tensile tests on this series of architectures were performed according to ASTM standard D3039[22] to determine the architecture-dependent responses of the material. Test samples were cut and tabs were bonded to the end of the specimen to create better gripping surfaces and reduce gripping damage (Fig. 6.) Specimens were 0.25 inch thick, 1 inch wide, and 8 inches long. The tests were conducted at a

rate of 0.05 inch/min (1 mm/min), while cross-head displacement and load along with digital image correlation (DIC) data were collected to obtain the strains occurring on the surface of the material.

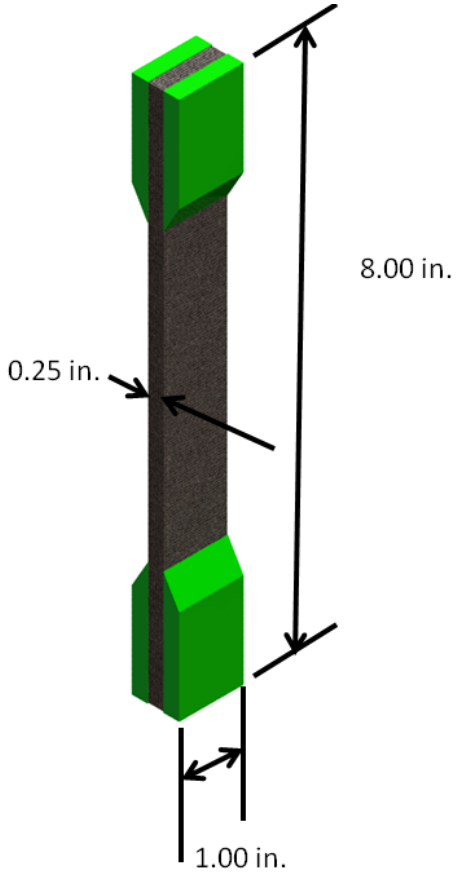

Fig. 6 Tensile samples prepared and tested per ASTM D3039[22]

5.2 Laterally Confined Compression Test

The LCC test was conducted on the 3-D woven architectures to determine the fiber tow shear strength. A standard compression test was modified by confining the sides of the samples to force a through-the-thickness shear failure of the samples. The test is only performed in through-the-thickness direction because this is the most likely failure plane for fiber tow shear failure. Three different orientations were tested: 0°, 45°, and 90°. Through-the-thickness testing for laminated composites results in plasticity in the matrix and large amounts of out-of-plane deformation. These tests do not mimic structural-level responses, which may trigger higher magnitude of failure modes. Therefore, through-the-thickness compression has been modified to include additional confinements. By loading a sample in the z direction (see Fig. 7), if movements in the y direction are prevented, the sample will form deformation in the x direction. This deformation causes a shear deformation in the fibers because the Poisson's effect is prevented from occurring. Figure 7 shows a simplified version of the test fixture. The specimens

used were 0.75 × 0.75 × 0.25 inch thick. Typically, unidirectional composites are forced to fail by a shear band formation; that is, by shearing the fiber tows. This kind of failure mode is typically seen during an impact or penetration of composite materials. Currently there is no ASTM standard for this test. Samples were run to failure with the load displacement shown in Fig. 7.

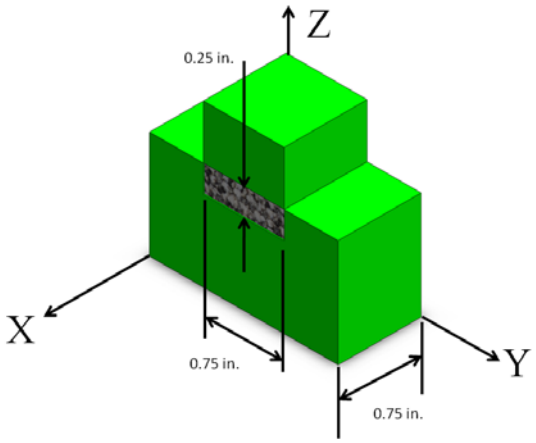

Fig. 7 LCC test specimen with simplified test fixture shown in green

6. Results and Discussion

6.1 Tensile Test Results and Discussion

6.1.1 Tensile Modulus:

Table 5 provides a comparison of the elastic modulus of the tested materials.

Table 5 Tensile modulus (Msi)

Configuration	0°	45°	90°
Base	3.22 ± 0.08	…	3.22 ± 0.08
3%	3.73 ± 0.11	1.14 ± 0.06	3.24 ± 0.07
6%	3.56 ± 0.21	1.08 ± 0.04	3.11 ± 0.16
10%	3.58 ± 0.04	1.15 ± 0.07	3.36 ± 0.18
12°	2.95 ± 0.06	1.25 ± 0.07	2.30 ± 0.04
20°	2.36 ± 0.08	0.93 ± 0.01	2.31 ± 0.02
60°	2.19 ± 0.07	0.97 ± 0.04	2.04 ± 0.09

The results shown in Table 5 indicate that the 3% Z-fiber architecture has the largest modulus of all the architectures presented here, including the 2-D laminate (Base). The 6% Z-fiber modulus is also very similar to the 3% and Base moduli. A decrease in modulus is observed as the amount of Z-fiber is increased (e.g., 10% Z-fiber) in the material. This is because the amount of in-plane

fibers is reduced to accommodate the increased percentage of Z-fibers, causing a decrease in the in-plane elastic modulus. In addition, more “defects” are likely introduced into the material with the increased amount of Z-fibers, which could contribute to the reduction in moduli. The layer-to-layer materials also show a significant degradation in the in-plane mechanical properties. For all of the tests, the 45° orientation acts as a shear test for the material, as there is no method by which the fiber tow bundles can transfer the load in the center of the specimen. The 12° samples have the highest modulus at the 45° orientation. For this architecture, all of the specimens in 0° and 90° orientations failed near the grips. The specimen failed locally at the location where the taper on the bonded tabs meets the sample. The 45° samples all failed locally in the gauge section and, therefore, observations of failure in these tests are fairly accurate.

6.1.2 Tensile Strength:

The tensile strength values obtained from the test are provided in Table 6.

Table 6 Tensile strength (ksi)

Configuration	0°	45°	90°
Base	3.22 ± 0.08	…	3.22 ± 0.08
3%	3.73 ± 0.11	1.14 ± 0.06	3.24 ± 0.07
6%	3.56 ± 0.21	1.08 ± 0.04	3.11 ± 0.16
10%	3.58 ± 0.04	1.15 ± 0.07	3.36 ± 0.18
12°	2.95 ± 0.06	1.25 ± 0.07	2.30 ± 0.04
20°	2.36 ± 0.08	0.93 ± 0.01	2.31 ± 0.02
60°	2.19 ± 0.07	0.97 ± 0.04	2.04 ± 0.09

The results indicate that the 6% and 10% specimens have the highest strength among the 3-D woven architectures. There are some higher deviations in the 6% samples than the 10%, which is likely due to manufacturing imperfections. One interesting finding is that the strength of 6% z architecture is very similar to that of the Base material. This indicates that the addition of 6% through-the-thickness reinforcement fiber does not affect or degrade the in-plane tensile properties. The strength of the layer-to-layer materials is relatively low except for the 12° in the 0° direction. For these architectures, the interlayer movement provides high-undulation angles in the fibers, causing higher stress concentrations. As the fiber tows are strained, the pulling effect results in large localized stresses as a result of the load not being applied along the tensile axis. Overall, the orthogonal (Z-fiber) architectures have a higher modulus and failure strength than the layer-to-layer architectures. A significant difference in material properties between the 2 architectures can be observed where the layer-to-layer is roughly two-thirds of the strength of the orthogonal samples. Stress-strain curves from the tensile experiments are shown in Fig. 8, which also shows the representative stress-strain plots after data reduction. The 0° and 90° orientations show a bilinear response characterized by an elastic portion with some deviation at higher strains followed by ultimate failure. The transition point in the bilinear response occurred at lower strains for the layer-to-layer architectures.

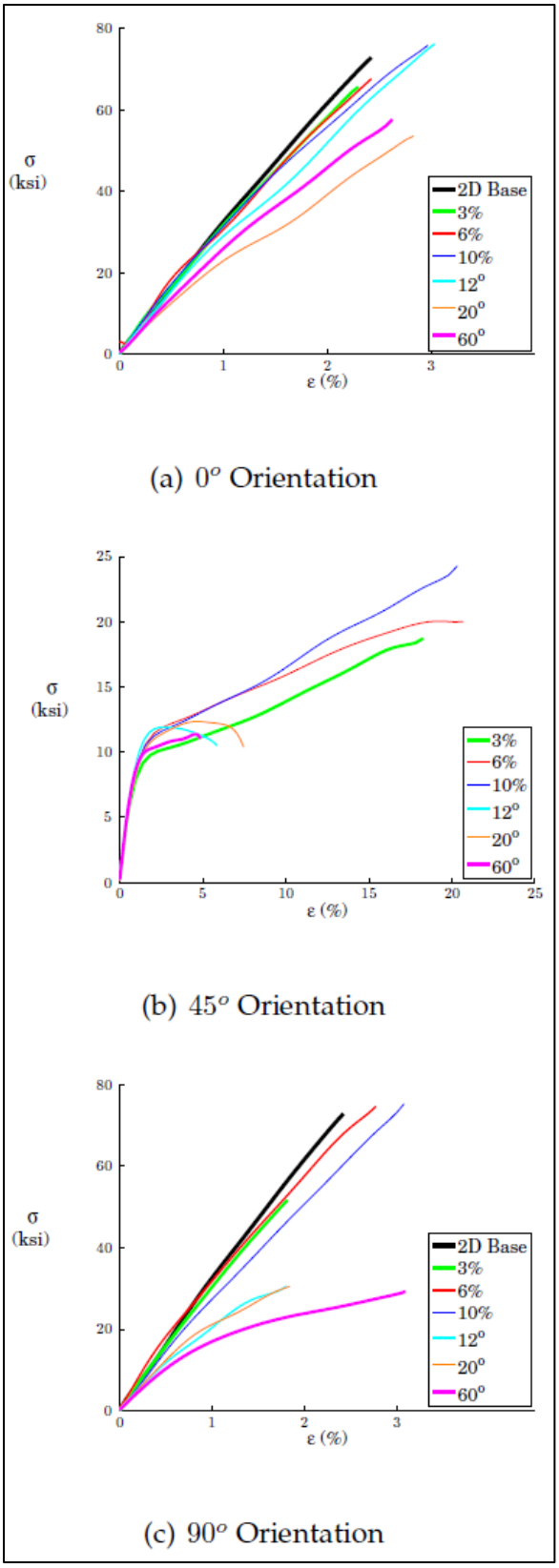

Fig. 8 Stress-strain curves from tensile experiments

6.2 Tensile Test Specimen Failure Analysis

The failed specimens were analyzed using a dye penetrant. Figure 9 shows the images of the specimens after failure and dye penetration. Each of the Z-fiber architectures shows periodic damage that occurs in the structure. The cracks in the specimens can be identified by the white lines in the images. Figure 10 shows the crack formations on the 45° orientation samples of the orthogonal specimens. This orientation was chosen because the surface cracks directly show all the different fiber tow bundles as they relate to the architecture. The periodicity on the surface of the samples relates to the location of Z-fibers in the architecture to illustrate that the architecture was overlaid on the picture to show the correlation.

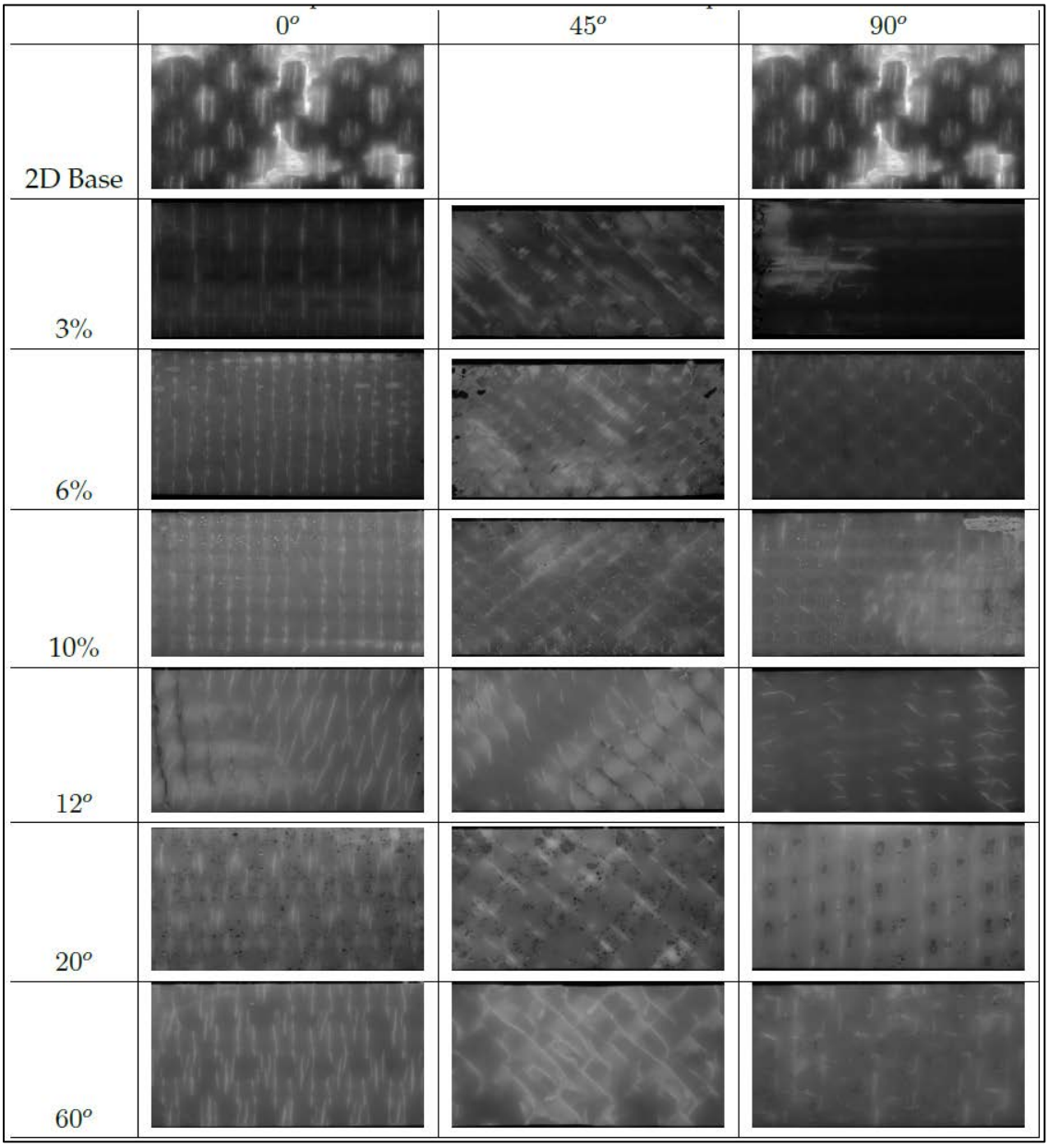

Fig. 9 Tension specimen cracks on the surface with dye penetrant

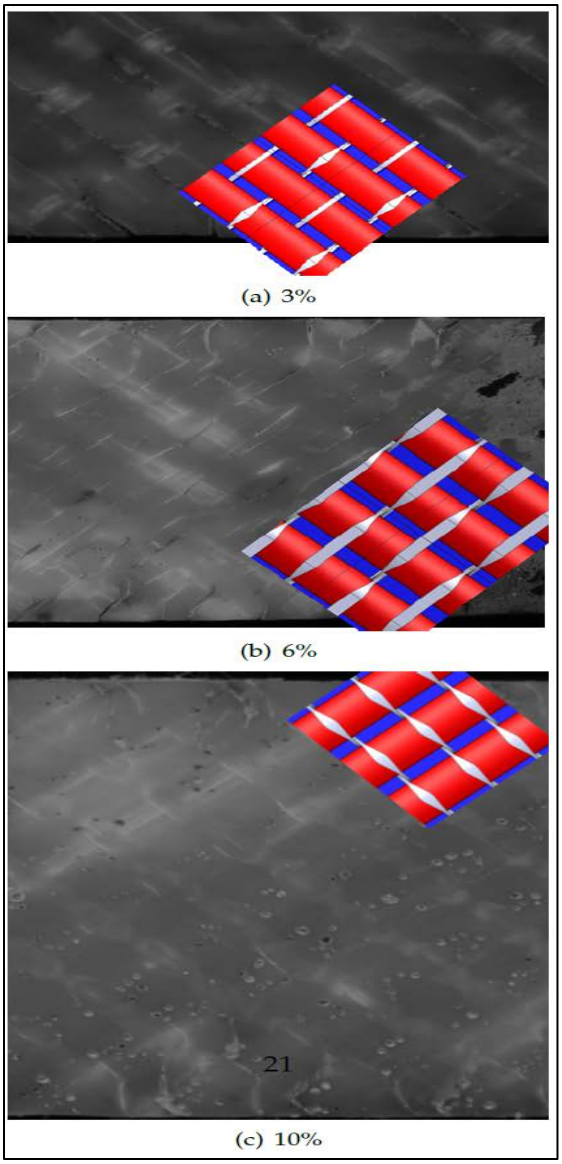

Fig. 10 Comparison of architectures regarding crack formaitons on the surface of Z-fiber specimens

The layer-to-layer architectures show some periodicity, but the surface failure is much more complicated due to the architecture. Unlike the Z-fiber architectures, the surfaces of the layer-to-layer materials do not have a rigid 0°–90° arrangement; hence it becomes much more difficult to identify the failure modes. The 12° material shows a clear path that the fibers follow while moving over the tow bundles. Instead of clear bands and lines that formed in the Z-fiber cases, the paths follow angles and the movement of the fibers as they move from one row to the next.

Additional details can be observed from the pictures of the idealized surfaces (Fig. 11). The other layer-to-layer materials show similar patterns to identify the cracks that occur on the surface.

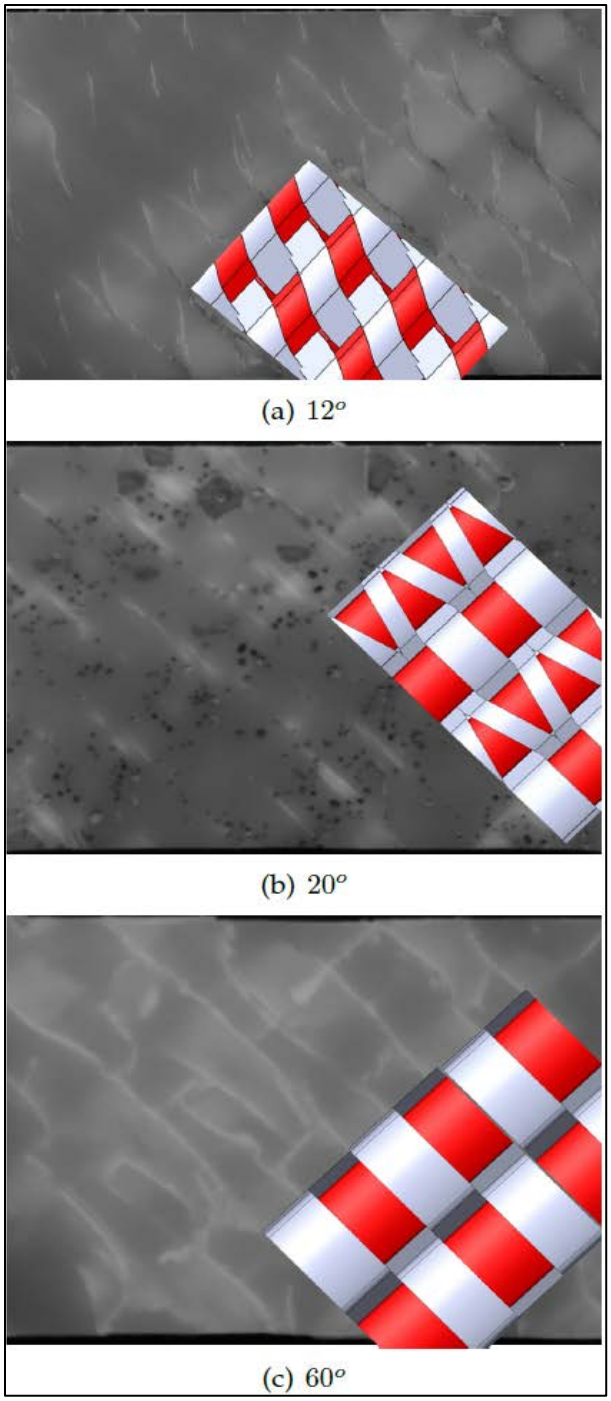

Fig. 11 Comparison of architectures regarding crack formations on the surface of layer-to-layer specimens

Most cracks are formed on the sides of a fiber tow bundle. The 45° samples do not have a direct load carrying path for any of the fibers, which is illustrated in Fig. 12. The fibers in the middle of the specimen are unable to carry the applied load directly, and therefore the failure localizes in the center because the load is carried predominantly in shear.

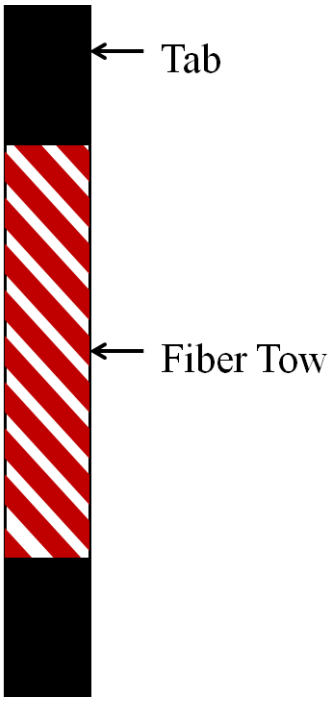

Fig. 12 Tension specimens with a 45° orientation, indicating the fiber tows unable to directly transfer the load

6.3 LCC Test Results and Discussion

Previously performed compression testing on 3-D woven materials at low and high rates has shown that there is a transition in failure mode that occurs at elevated rate loading.[23] At these rates and in actual impact scenarios, penetration acts as if the material is confined from expanding and shear bands occur in the material.[24] Therefore, a new test method was developed to investigate the response of the material and excite these failure modes quasi-statically. The punch shear method works by punching a hole in a composite and looking at the shear failure angles that are formed in the material.[25] The angle of the band associated with shear failure has also been investigated previously to determine the effective failure envelope that can be formed.[26] However, interpretation of the results of these tests is often very difficult. Based on the maximum load and the cross-sectional area, the effective normal stress acting on the surface was computed to determine the effective strength of these materials, shown in Eq. 1.

$$\sigma_c = \frac{F_{max}}{A}, \tag{1}$$

where F_{max} is the maximum load and A is the cross-sectional area. These values have been computed and are reported in Table 7. The 2-D plain-woven fabric had the highest compression strength of all the material tested. The 45° specimens are difficult to compare because cracks do

not form readily in these samples, as the weak planes typically positioned in the 0° and 90° orientations. The 6% Z-fiber samples seemed to have the highest consistent through-the-thickness strength of all the architectures. The layer-to-layer materials performed lower in all orientations; however, this is expected because the material is more likely to try and flatten out when compressed. It appears the material is actually consolidating under initial loads. This could be because of the complex architecture, which results in higher undulations that in turn allow for layer matrix plasticity. The representative stress-strain plots obtained from the LCC test after data reduction are shown in Fig. 13.

Table 7 Compressive strength (ksi) obtained from LCC test

Configuration	**0°**	**45°**	**90°**
Base	102.4 ± 6.1	…	102.4 ± 6.1
3%	95.9 ± 7.7	86.0 ± 4.3	86.3 ± 5.5
6%	91.4 ± 7.5	89.3 ± 3.4	92.4 ± 5.6
10%	91.9 ± 4.7	93.8 ± 1.1	79.5 ± 7.7
12°	95.4 ± 2.5	78.7 ± 2.3	73.9 ± 1.3
20°	63.4 ± 2.9	63.7 ± 1.5	66.7 ± 2.9
60°	71.0 ± 2.4	69.3 ± 3.2	55.6 ± 3.0

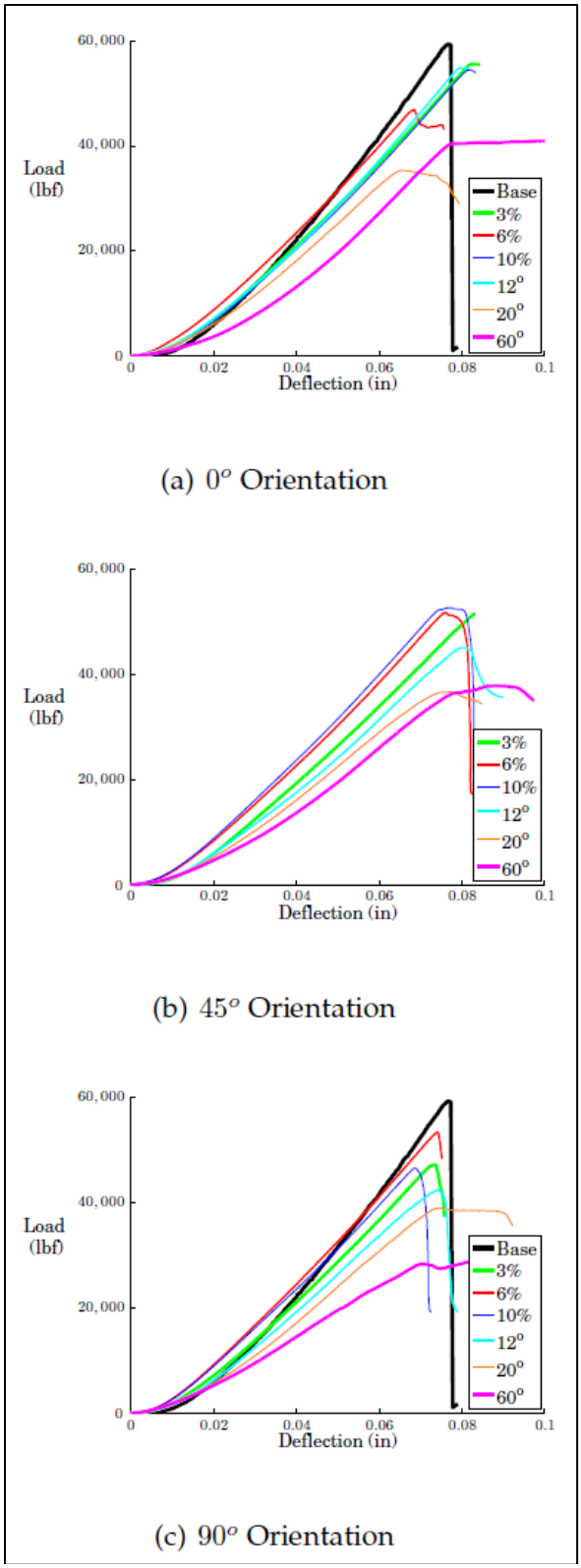

Fig. 13 Load vs. deflection curves from LCC experiments

6.4 LCC Test Specimen Failure Analysis

LCC posttest failure analysis was conducted using Zyglo ZL-67 dye penetrant, which was applied to the surface for 10 min. Excess penetrant was removed with acetone, allowing the penetrated cracks to remain visible under a black light. Surface images of the samples were obtained to identify the failure surfaces that formed in the different materials. The scanned images are shown in Fig. 14. The specimens were optically observed due to the high damage density, as the dye penetrant did not yield any useful data. As discussed earlier, the cracks that form in the 45° specimens form at an angle that does not align with in plane fibers and therefore the conclusions are difficult to draw for these samples.

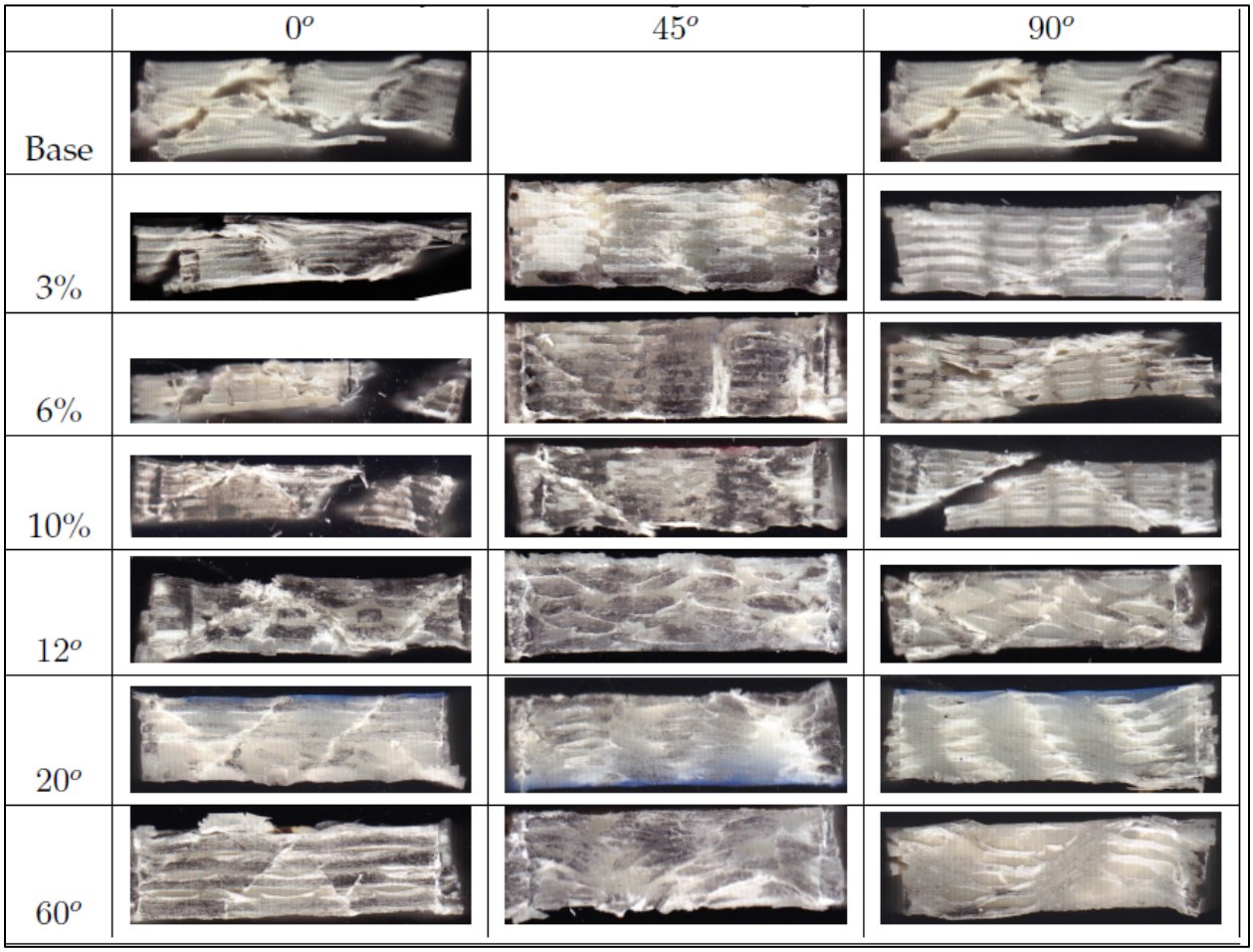

Fig. 14 LCC specimens after testing

The 2-D woven samples showed multiple shear bands that form in the samples. On a thicker sample, there is typically a single shear band formation. However, due to the relatively thin 2-D specimens, multiple cracks are formed. This pattern was similar in all of the Z-fiber samples with multiple shear fractures. Most of the samples showed a large amount of energy release, as the samples typically separated into multiple pieces. This energy release was observed during the test through a very loud noise. The Z-fiber samples showed clear failure angles. While the

layer-to-layer samples produced failure, the failure surfaces were not straight forward, as the path of the fibers changed through the depth of the sample. The 20° and 60° samples showed shear angles that coincided with naturally found patterns in the consolidated architecture, often following the edge of the warp or weft tows. These samples did not display as much energy dissipation as the Z-fiber architecture. The samples were still mainly intact after testing, with cracks running through the samples, and there was very little acoustic emission at the onset of failure. This can further be shown by examining the load deflection curves in Fig. 14, which show the load plateaus, but additional deflection is observed.

To further understand the experiment, the average angle of the shear bands was measured and reported in Table 8. If a single shear band were formed, the components could easily be broken down into the effective components acting on the fiber tow bundle. However, with multiple cracks this analysis becomes more difficult for accurate results. The orthogonal Z-fiber samples were found to have angles similar to those formed in the 2-D woven samples. The 20° and 60° samples were found to have higher angles of failure. The maximum strength was then broken down to determine the effective shear stress and the normal stress on the surface of the crack using a Mohr's circle analysis and based on the average angle formed in the samples. The resulting normal and shear components can be determined from the effective components.

$$\sigma_n = \sigma_c \cos^2 \theta \tag{2}$$

and

$$\tau = \frac{1}{2}\sigma_c \sin 2\theta, \tag{3}$$

where σ_c is the compressive stress, σ_n is the normal stress on the surface, and τ is the shear stress on the failure surface. The angles have been determined from the pictures in Fig. 14 with the average angles being reported in Table 8.

Table 8 Shear angle

Configuration	**0°**	**90°**
Base	44.8 ± 1.4	44.8 ± 1.4
3%	39.6 ± 6.2	41.9 ± 7.6
6%	42.7 ± 6.7	43.4 ± 3.2
10%	39.2 ± 4.8	37.6 ± 8.6
12°	40.5 ± 4.7	42.3 ± 4.3
20°	46.4 ± 5.9	53.0 ± 3.8
60°	52.2 ± 5.5	46.2 ± 0.4

The average components were determined from the stresses and are shown in Table 9. This table shows that the Z-fiber samples have larger normal and shear stresses than those of the layer-to-layer architectures. The orthogonal Z-fiber specimens typically had an angle of around 40°, which produces a similar shear and normal force. The layer-to-layer architectures had larger angles that formed in the samples, except for the 12° architectures. These higher angles produce

larger shear forces than normal forces. These results are similar to that of a punch shear test in a sample where there is more of a pure shear occurring on the surface of the parts. Overall, the stress components of the Z-fiber composite produce similar results to those observed from 2-D plain woven fabric. Therefore, the insertion of through-the-thickness reinforcement from Z-fibers produces only a small amount of effect on the compression shear response of these materials.

Table 9 Component forces (ksi)

Configuration	0°		90°	
	σ_n	τ	σ_n	τ
Base	51.5	51.2	51.5	51.2
3%	53.1	47.7	51.3	42.4
6%	49.3	45.6	48.8	46.2
10%	55.2	45.0	50.0	38.4
12°	55.2	47.1	40.4	36.8
20°	30.2	31.7	20.8	30.9
60°	26.7	34.4	26.6	27.8

7. Conclusion

Quasi-static tests were performed on each of the various different 3-D woven architectures so that a comparison of mechanical properties could be made. The results showed that the Z-fiber architecture performs in a similar manner to 2-D woven composites with little degradation in mechanical properties. The layer-to-layer materials showed larger degradations in material properties except for in the shearing of the material, where it performed the best in plane. Based on the data, 6% Z-fiber architecture may be the “best” architecture to provide both strength and stiffness based on the results provided here. It shows that there may be an optimum amount of Z-fiber that can be inserted into a material for property enhancement. It will have similar reasons to those for particle reinforcement ideas. Although the layer-to-layer architectures were poor in tensile and compression, the energy absorption capabilities of these materials may be beneficial in certain applications.

8. References

1. Kang TLS. Effect of stitching on the mechanical and impact properties of woven laminate composites. Journal of Composite Materials. 1994;28(16):1574–1587.
2. Sharma S, Sankar B. Effect of stitching on impact and interlaminar properties of graphite/epoxy laminates. Journal of Thermoplastic Composite Materials. 1997;10:241–253.
3. Huang H, Waas A. Compressive response of z-pinned woven glass fiber textile composite laminates. Composites Science and Technology. 2009;69:2331–2337.
4. Mouritz A. Compression properties of z-pinned sandwich composites. Journal of Materials Science. 2006;41:5771–5774.
5. Cartie D, Partridge I. Delamination resistant laminates by Z-fiber pinning. Composites: Part A. 2005;36:55–64.
6. Cox B, Dadkhah M. The macroscopic elasticity of 3D woven composites. Journal of Composite Materials. 1995;29:785–819.
7. Clay S, Pommer A. Z-pin stubble technology advanced research (zs-tar). Wright-Patterson Air Force Base (OH): Air Force Research Laboratory (US); 2008. Report No.: AFRL-RB-WP-TR-2008-3107.
8. Lee B, Leong K, Herszberg I. Effect of weaving on the tensile properties of carbon fibre tows and woven composites. J Rein Plastics and Comp. 2001;20:652–670.
9. Lee L, Rudov-Clark S, Mouritz, A, Bannister M, Herszberg I. Effect of weaving damage on the tensile properties of three-dimensional woven composites. Composite Structures. 2002;57:405–413.
10. Yushanov S, Bogdanovich A, Mohamed M. Manufacturing and property analysis of a novel class of 3-D woven composites. Journal of Thermoplastic Composite Materials. 1999;12(1): 70–82.
11. Kamiya R, Cheeseman B, Popper P, Chou T. Some recent advances in the fabrication and design of three-dimensional textile preforms: a review. Compos Sci Tech. 2000;60:33–47.
12. Mouritz A, Bannister M, Falzon P, Leong K. Review of applications for advanced three-dimensional fibre textile composites. Composites: Part A. 1999;30:1445–1461.
13. Herakovich C. Mechanics of Fibrous Composites, 2nd ed. New York: McGraw-Hill; 1998.
14. Zhou Y, Pervin F, Biswas M, Rangari V, Jeelani S. Fabrication and characterizationof montmorillonite clay-filled SC-15 epoxy. Materials Letters. 2006;60:869–873.

15. Justusson B, Yu J, Chen A, Chian-Fong Y. Mechanical testing of 3D fabric composites and their matric material SC-15. Aberdeen Proving Ground (MD): Army Research Laboratory (US); 2012 Nov. Report No.: ARL-TR-6245. Also available at: http://www.arl.army.milarl reports/2012/ARL-TR-6245.pdf.

16. Chen R, Dong C, Liang Z, Zhang C, Wang B. Flow modeling and simulation for vacuum assisted resin transfer modling process with the equivalent premeability methods. Polymer Composites. 2004;25(2):146–164.

17. ASTM D2734-94. Standard test method for void content of reinforced plastics. West Conshohocken, PA: ASTM International; 2003.

18. Leong K., Lee B, Herszberg I, Bannister M. The effect of binder path on the tensile properties and failure of multilayer woven CFRP composites. Composites Science and Technology. 2000;60:149–156.

19. Gu H, Zhili Z. Tensile behavior of 3D woven composites by using different fabric structures. Materials and Design. 2002;3:671–674.

20. Tan P, Tong L, Steven G, Ishikawa T. Behavior of 3D orthogonal woven CFRP composites part I: experimental investifation. Composites: Part A. 2000;31:259–271.

21. Callus P, Mouritz A, Bannister M, Leong K. Tensile properties and failure meachanisms of 3D woven GRP composites. Composites: Part A. 1999;30:1277–1287.

22. ASTM D3039. Standard test method for tensile properties of polymer matrix composite materials. West Conshohocken (PA): ASTM International; 2014.

23. Pankow M, Salvi A, Waas A, Yen C, Ghiorse S. Split Hopkinson pressure bart testing of 3D woven composites. Composites Science and Technology. 2011;71(9):1196–1208.

24. Sun Y, Wang G. Compressive response of UHMWPE/vinyl ester 3D orthogonal woven composites at high strain rates. Advance Materials Research. 2010;97–100:522–525.

25. Manzella A, Gamma B, Gillespie J Jr. Effect of punch and specimen dimensions on the confined compression behavior of S-2 glass/epoxy composites. Composite Structures. 2011;93(7):1726–1737.

26. Gillespie J, Gamma B, Cichanowski C, Xiao J. Interlaminar shear strenght of plain weave S-2-glass/SC79 composites subjected to out-of-plane high strain rate compressive loadings. Composites Science and Technology. 2005;65(11–12):1891–1908.

List of Symbols, Abbreviations, and Acronyms

3-D	three-dimensional
ARL	US Army Research Laboratory
DIC	digital image correlation
LCC	laterally confined compression
RUC	representative unit cells
T.E.A.M	Textile Engineering and Manufacturing
VARTM	vacuum-assisted resin transfer molding

1 DEFENSE TECHNICAL
(PDF) INFORMATION CTR
DTIC OCA

2 DIRECTOR
(PDF) US ARMY RESEARCH LAB
RDRL CIO LL
IMAL HRA MAIL & RECORDS MGMT

1 GOVT PRINTG OFC
(PDF) A MALHOTRA

3 DIR USARL
(PDF) RDRL WMM A
A QUABILI
RDRL WMM B
C YEN
M PANKOW

.